Fundamental understanding of the deformation mechanism and corresponding behavior of RB-SiC ceramics subjected to nano-scratch in ambient temperature

Zhipeng Li[a], Feihu Zhang[a*], Xichun Luo[b], Yukui Cai[b]

[a] School of Mechatronics Engineering, Harbin Institute of Technology, Harbin, China

[b] Centre for Precision Manufacturing, DMEM, University of Strathclyde, Glasgow, UK

Abstract

To get insight into nano-scale deformation behavior and material removal mechanism of RB-SiC ceramic, nanoscratch experiments were performed using a Berkovich indenter. Structure changes in chips and subsurface deformation were characterized by means of Raman spectroscopy. The result shows that the SiC phase underwent amorphization in ductile chips, while no amorphous feature can be observed in brittle chips and substrate within scratch groove. The following estimated stress surround the indenter reveals that amorphous deformation in ductile chips is governed by tangential stress (above 95 GPa), whereas the dislocations-based substrate deformation mechanism was dominated by normal stress. In the end, the effects of normal load and scratching velocity on the scratch behavior including scratch residual depth, elastic recovery and friction coefficient that related to RB-SiC ceramic deformation mechanism were also analyzed. With the increase of normal load, the deformation mechanism transfers from ductile to brittle fracture mode and cause the decrease of elastic recovery and the increase of residual depth and friction coefficient. Furthermore, the increased high density of dislocations as a result of the increased scratching velocity give rise to the increase of scratch hardness, which

finally result in the increase of elastic recovery and decrease of residual depth and friction coefficients. This study contributes a new understanding of the brittle material deformation mechanism during a nano-scale scratching process.

Key words: RB-SiC ceramic; amorphization; dislocation; brittle fracture; scratch behavior.

Nomenclature			
h	Scratch depth	τ	Interfacial tangential stress
α	The centerline-to-face angle of Berkovich indenter	σ	Interfacial normal stress
h_d	Pile up of residual scratch groove	γ	Material flow orientation
A	The contact area between scratch groove and Berkovich indenter	k	Modified coefficient
F_N	Normal force	a	Width of scratch groove
F_T	Lateral force	$\dot{\varepsilon}$	Strain rate
D, m	Empirical coefficients	E_r	Elastic recovery
v	Scratch velocity	H_r	Residual depth
μ_a	Adhesion coefficient	μ_p	Ploughing coefficient
s	Shear strength	σ_y	Yield stress
H	Vickers hardness	E	Elastic modulus

1. Introduction

Reaction bonded silicon carbide (RB-SiC) ceramic is being considered as a prime material candidate for large mirrors of space or ground based telescopes due to its combination of mechanical properties of high strength, high chemical inertness, enhanced radiation stability and thermal shock resistance [1,2]. Such applications

have strict requirements on surface tolerance, surface finish and surface/subsurface damage. However, intrinsic high hardness and brittleness characteristics of ceramics make fracture defects are inevitable in traditional grinding process. Hence, it is desirable to fabricate brittle material in ductile removal mode, through which an optical quality surface with little or even no surface and subsurface damages is expected to be obtained [3, 4]. Understanding the material removal mechanism and critical transition from ductile to brittle fracture (DTB) has therefore been a subject of significant interest [5-8].

Actually, it is general acceptable that no matter how brittle of the material, it has some level of ductility if the undeformed chip thickness is below a certain critical limit in machining [9, 10]. Several researchers, thereafter, attempts to quantify the critical depth of DTB with material physics properties [3] or a variety of different contact loading conditions such as pressure loading [11], scratching [12,13], nanoindentation [14] and nanometric cutting [9,15]. Meng et al. [12] performed nanoscratch tests on 6H-SiC and found the critical depth for DTB is around 75 nm when the applied normal load is about 12.2 mN. However, Cao et al. [13] got that 0.08 μm is the critical depth for ductile to brittle transition in the conventional scratch test of SiC ceramic. They also found that with the assist of ultrasonic vibration the depth of cut can increase around 56.25% than conventional scratch to 0.125 μm. Besides, in the nano-indentation of 6H-SiC (0001) Yin et al. [14] found that the no cracks were occurred when the normal load is up to 400 mN, which has controversy with the findings in reference [11]. Currently the critical depth of cut for SiC is still inconclusive because its value is determined by several parameters pertaining to intrinsic material properties, tool geometry, processing parameters and removal mechanism. The key factor to reveal the difference of critical depth lies in

understanding the corresponding deformation mechanism induced by different machining conditions. Especially for RB-SiC ceramics which compose of Si phase, SiC phase and phase/grain boundary to lead to more complicated deformation mechanism than a single crystal material. To date, the deformation mechanisms of SiC materials were mainly including, high pressure phase transformation [16], dislocations slip [17] or amorphization [15, 18]. For instance, Yan et al. [17] found that dislocations were the primary ductile mechanism of 6H-SiC grain in the subsurface of diamond turning RB-SiC ceramics. No amorphous phase peaks can be identified in Raman spectrum. However, Zhang et al. [15] proposed that amorphization (High-Pressure Phase Transformation, HPPT) occurred for both SiC and Si phases in the outmost layer during micro grinding of RB-SiC ceramics according the results of X-ray diffraction (XRD) detection [10]. Similarity, Xiao et al. [16] also claimed that HPPT accompanied Frank partial dislocations and basal plane edge dislocations indeed took place in the molecular dynamic (MD) simulation of diamond turning of 6H-SiC. On the contrary, Goel et al. [19, 20] insisted that HPPT will not happen in the nano-machining of SiC since the maximum pressure remains less 100 GPa in their MD simulations using the Tersoff potential. Wu et al. [6] concluded that in the nano-scale machining of 6H-SiC, the ductile-regime can be achieved by either the structural transformation (Wurtzite structure to an amorphous structure), or by the migration of dislocations (in the case of plan-strain deformation), or by a combination of them. From the above mentioned studies, it can be concluded that the researches on the DTB transition depth and deformation mechanism in diamond machining of SiC are inconclusive. Therefore, this paper focuses on the investigation of the removal mechanism of RB-SiC ceramics through analyzing the structure changes in chips and subsurface substrate.

It is known that nano-scratch technique was the most effective and common method to investigate the material mechanical properties and removal behavior in abrasive machining [21-23]. The material deformation/fracture patterns arising from the surface morphologies of the scratch provide primary information for determining material removal behavior. In the current work, therefore, a series of nano-scratch tests were performed on RB-SiC to investigate the material removal mechanism based on the scanning electron microscopy (SEM) observation and Raman measurement of residual scratch groove and chips. The tangential and normal stresses around the Berkovich indenter were analyzed to explain the difference deformation mechanism emerged in ductile chips and subsurface of substrate. Finally, based on the deformation mechanism under different process conditions, the effect of scratch speed and normal load on removal behavior such as residual depth, elastic recovery and scratch force were discussed. This research is expected to give a further insight into the deformation mechanism in the nano-scratch of RB-SiC ceramic, and determine the inner link between material deformation mechanism and removal behavior.

2. Experiments

2.1 Material properties

The RB-SiC ceramic used in this investigation was fabricated by Goodfellow Cambridge Limited. The size of specimen dimension was 12.5 mm×12.5 mm×5 mm and its main physical characteristics were listed in **Table 1**. To minimize the defects induced by sintered process, the received samples were polished with diamond of 1～3 μm grit size until the surface roughness (Ra) less than 5 nm as measured with AFM.

Table 1. The physics properties of RB-SiC

Workpiece	RB-SiC
Elastic modulus E (GPa)	390
Vickers hardness H (kg/mm^{-2})	3000
Compressive strength (MPa)	2000
Fracture toughness K_{IC} (MPa·m$^{1/2}$)	4.0
Density ρ (g/cm^3)	3.1
Passion ratio υ	0.24
Average diameter (μm)	10

2.2 Experimental setup

All the nano-scratching tests were conducted on the Nano Indenter G200 (MTS Systems Corp.) (**Fig. 1a**), employing a standard diamond Berkovich indenter with a tip radius about 130nm, as shown in **Fig. 1b.** In this study, the Berkovich indenter was oriented in an edge leading in the scratch direction (**Fig. 1c).** This machine equipped with a transducer with a normal force/displacement sensor and two lateral force/displacement sensors, which can acquire the lateral force and scratch depth in real time.

To insight the effect of normal load and scratching velocity on removal behavior, scratch depth/ elastic recovery ratio and friction, a serials of constant and continuous loading mode scratch tests were performed with applied normal load ranging from 0 mN～50 mN and scratching velocity within 1 μm/s～2000 μm/s. Besides, in order to obtain a statistically reliable data at least three scratches were made at each set. All tests were carried out at the temperature about 23℃. After the scratch experiments, for the purpose of characterizing the material removal behavior and fracture pattern,

the topography of the scratch groove was observed by a scanning electron microscope (SEM). A J-Y HR 800 Raman system equipped with an argon ion laser with 488 nm line excitation wavelength was employed to uncover structure changes in the debris and subsurface of substrate. The laser beam was focused to a spot size of 0.8 μm in diameter. After the non-contact examination, the specimens were cleaned in acetone for 10 min using an ultrasonic washer. The three-dimensional scratch groove topography including the residual depth and the height of pile-up along grooves sides were obtained using an atomic force microscopy (AFM) (Germany Bruker, dimension icon).
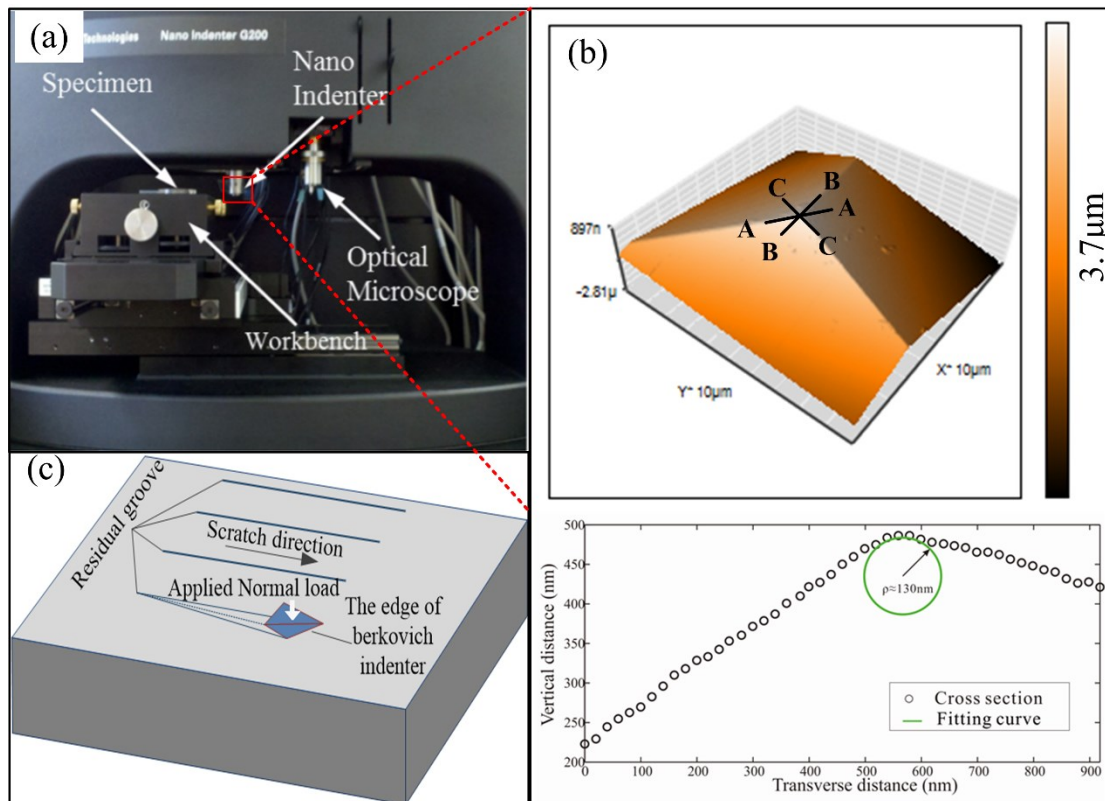
Fig. 1. (a) The apparatus of Nano indentor G200 used for scratching tests (b) The detail of 3D topography of Berkovich indenter and tip radius profile measured by AFM (c) A schematic of nano-scratch process.

3. Results and discussion

The effects of several parameters such as the applied normal load, scratching velocity on the material removal mechanism, elastic recovery, residual depth and scratch friction of the studied RB-SiC ceramic are discussed in the following sections.

3.1 Effect of normal load and scratching velocity on material removal mechanism

Fig. 2 shows the residual topography after nano-scratch with ramp normal loading condition which increased linearly from 0 to 50 mN. From the traces of residual scratch morphology, it can be identified that the deformation behavior of RB-SiC ceramic is divided into three different regimes based on the surface cracks in a typical scratch process. As shown in **Fig. 2a**, when the normal load increases to about 2 mN, the deformation behavior entrances the plastic deformation stage that the surface topography appears smooth and no cracks can be observed. After that, as the load increases up to about 20 mN, the micro-cracks were emerged within the grooves as depicted in **Fig. 2b** and **c**. At the last regime, with the continues increase of normal load, the successive crack comes into being along the grooves and some lateral cracks propagated to the sides of the groove which might leading the material removed in macroscopic chipping. The residual topography results reveal that the deformation behavior of RB-SiC ceramic is strongly dependent on the normal load (contact stress) level. In addition, it is very interesting to note that the phase boundary and grain boundary play an important role in the propagation of crack as shown in **Fig. 2e** and **f**. As shown in **Fig. 2e**, the crack is blocked at the interface of the Si /SiC phase boundary or SiC/SiC grain boundary.

Fig. 3 shows the typical scratch topography inflicted with varied scratching velocity from 1 μm/s～2000 μm/s under the normal load of 10 mN. For scratch groove interior, the micrographs did not show an obvious difference between each

other, except some micro-cracks occurrence when the scratch speed at 1 μm/s (**Fig. 3a**). However, the AFM measurement results (shown in section **3.2**) exhibit that the residual depth and width of the scratch grooves decrease with the increase of scratching velocity (The reason will be discussed in Section **3.2**).
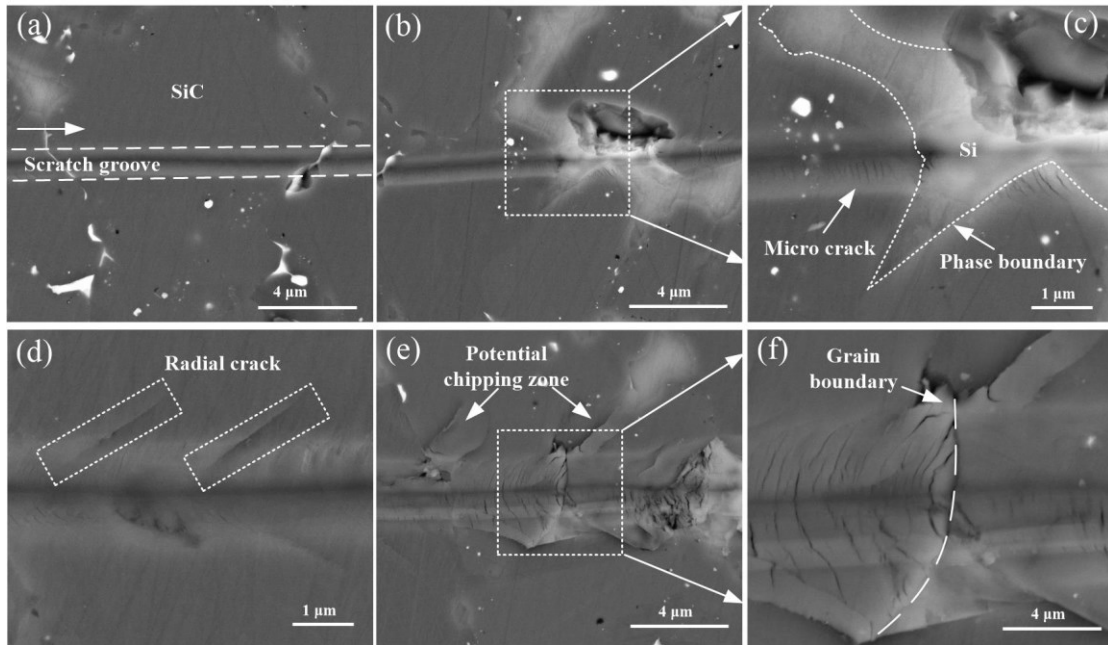
Fig. 2 Surface topography corresponding to the different removal stage with continuous load mode.
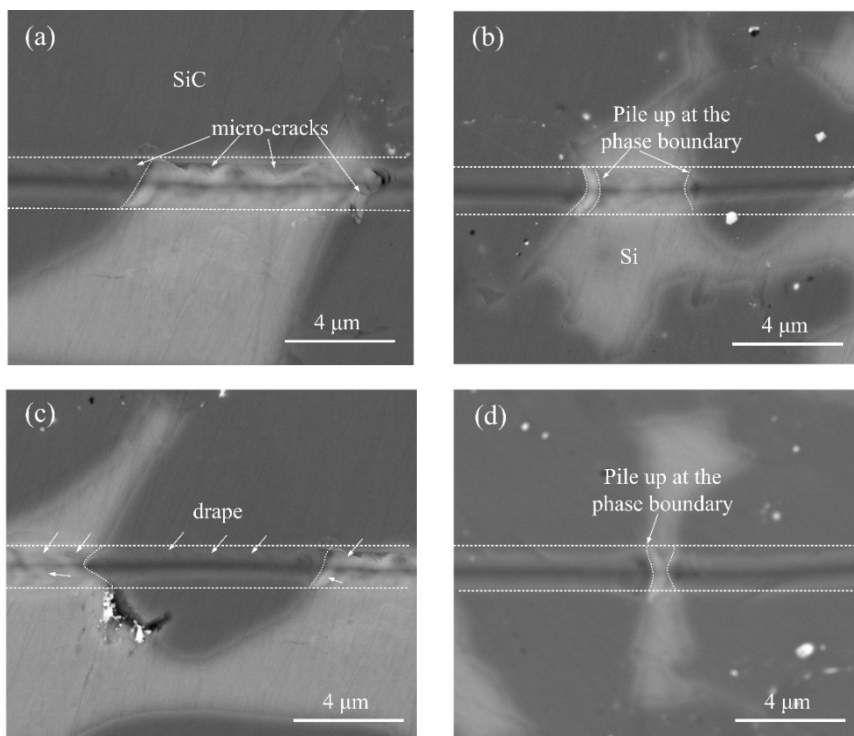
Fig. 3. Surface topography with different scratching velocity (a) 1 μm/s;(b) 500 μm/s;(c) 1500 μm/s (d) 2000 μm/s.

3.2 Structural analysis

Raman spectroscopy can be used to distinguish the structural changes in chips and substrate of RB-SiC ceramics induced by the scratching process. As shown in **Fig. 4a**, the Raman spectrum obtained before scratching, indicates that RB-SiC ceramics are mainly composed of Si-I phase with diamond structure (515 cm^{-1}) and 6H-SiC phase with hexagonal structure (600-1000 and 200-600 cm^{-1} region) [24]. The weak bands at the points of 145 cm^{-1}, 245 cm^{-1} ascribe to the folded modes of transverse acoustic (FTA) of 6H-SiC at $q/q_0=1/3$ and $q/q_0=2/3$ (q is wave vector), respectively. After scratching, if SiC or Si did not change its structure, the Raman spectra would totally reversible. However, the spectrum collected from ductile debris **D-1** (**Fig. 4b**) shows a significant broadband peak at 802 cm^{-1}, which can be assigned to heavily disordered SiC [24, 25]. In addition, another broadband associated with C-C bonds in the region of 1300-1600 cm^{-1} was detected. This is closely related to the characteristics of disordered sp^2 bonded arrangements. In general, these evidences revealed that in the ductile chips, high pressure phase transformation (amorphization) of SiC, indeed occurred during scratching with normal load of 30 mN. Whereas, in contrast, the Raman spectrum collected from the inside of residual groove (**Position 1**) or brittle fracture chips (**D-3**) (**Fig. 4d**) shows no evidence of amorphous pattern of SiC as illustrated in **Fig. 4b.** Therefore, it can be concluded that amorphous transformation took place in SiC grain during the ductile chips formation, while plasticity response of substrate most likely originates from the dislocation mobility. Such phenomenon has also been proved in our previous observation using transmission electron microscope [26], which showed that dislocations accompanied

with stacking faults were the main defects in subsurface of substrate. It is known from the theory of the plasticity that the contact stress between indenter determines the deformation mechanism. Thereby, the interfacial tangential stress and normal stress around the indenter will be estimated in the following section.

Apart from the SiC grain, it should be noted that a broadband located at 470 cm^{-1} arise on the spectrum of debris (**D-2**) and in grooves (**Position 2**), signifying Si has been partially transformed into an amorphous state. Another interesting observation from **Fig.4b** is the split peaks at the Raman shift of 515 cm^{-1} and 533~537cm^{-1}, which due to the non-uniform distribution of stress as a result of the plastic deformation of dislocations [27, 28]. Under the influence of the anisotropic stress of Si three-fold degeneracy phonon modes at Brillouin zone q=0 was broken, resulting in the split of different phonon frequencies.
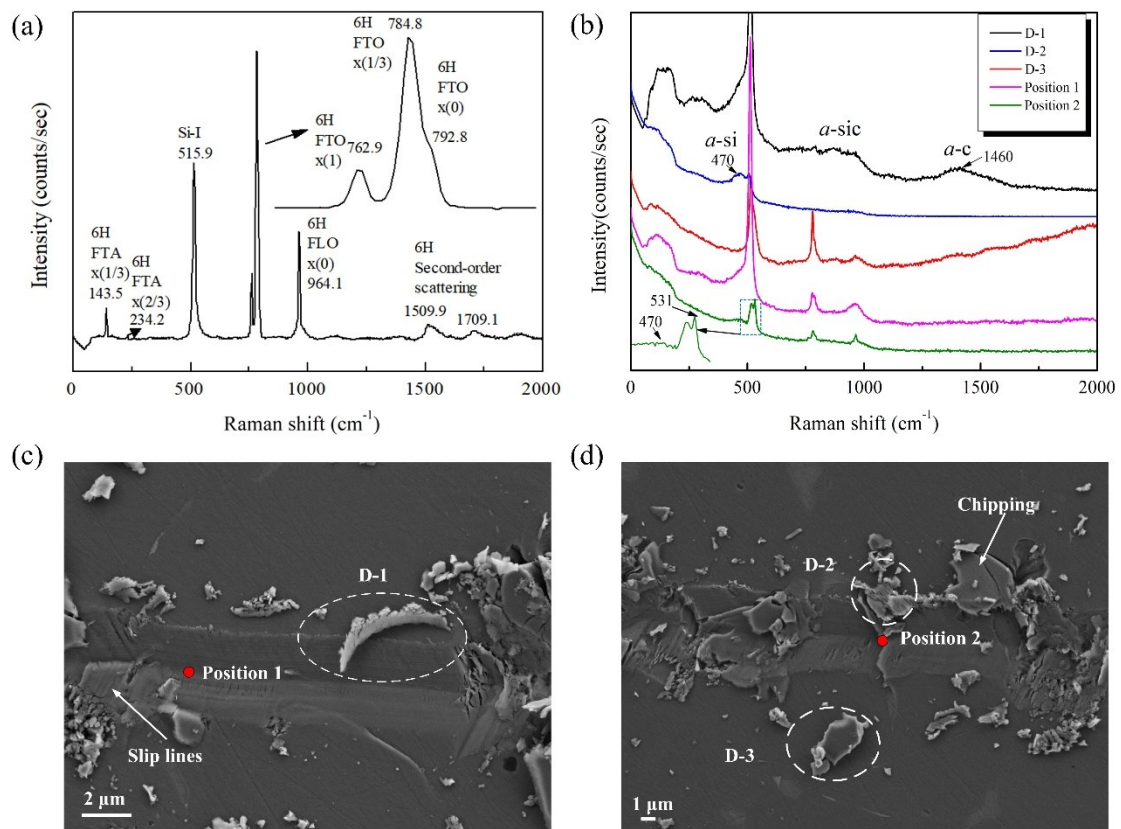
Fig. 4. Raman spectra collected from (a) original structure of RB-SiC ceramics (b) the debris and SiC grains present within and away from the scratch grooves as shown in (c) and (d).

3.3 Stress analysis

In this part, the normal stress and interfacial tangential stresses around the indenter were estimated, which can be used to explain the foregoing phenomenon of the different deformation mechanism in chips and substrate within scratch grooves.
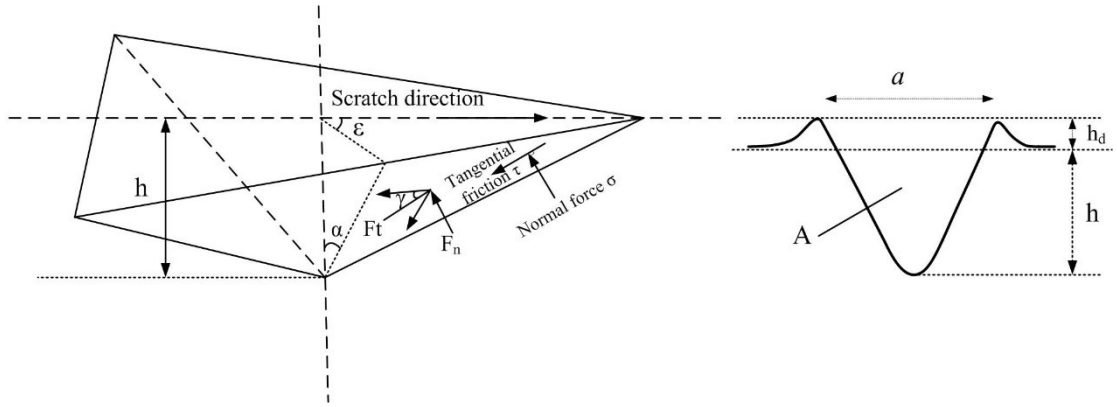
Fig. 5. The schematic of forces on the contact area (a) and the cross section of residual scratch groove (b).

Fig. 5 shows the contact area and cross section of residual scratch groove. The surface of one face of the Berkovich indenter for a height h is:

$$A = \frac{\sqrt{3}\tan\alpha}{\cos\alpha}h^2 + \frac{ah_d}{2\cos\alpha} \tag{1}$$

$$h = \frac{a}{2\sqrt{3}\tan\alpha} \tag{2}$$

Where $\alpha = 65.3°$ for a Berkovich indenter.

The measured normal force F_N and lateral force F_T can be expressed as [29]:

$$F_N = 2\sin\alpha F_n - 2\sin\gamma\cos\alpha F_t \tag{3}$$

$$F_T = 2(\cos\varepsilon\cos\alpha F_n + \sin\varepsilon\cos\gamma F_t + \cos\varepsilon\sin\alpha\sin\gamma F_t) \tag{4}$$

If we assume that the normal stress and interfacial tangential stress oriented at an angle relative to the horizontal are applied to two frontal indenter faces. So the relationship between the interfacial tangential stress τ/normal stress σ, angle γ, F_N and F_T can be given by [30]:

$$\tau = \frac{1}{A} \frac{\sin\alpha F_T - 1/2\cos\alpha F_N}{\sqrt{3}\cos\gamma\sin\alpha + \sqrt{1-\cos^2\gamma}} \tag{5}$$

$$\sigma = \frac{F_T}{A\cos\alpha} - \frac{\tau}{\cos\alpha}(\sqrt{3}\cos\gamma + \sin\alpha\sqrt{1-\cos^2\alpha}) \tag{6}$$

According to Eqs. (5) and (6), the stress calculated in this manner is not a unique solution, but varies with material flow orientation γ. **Fig. 6** shows how the normal pressure and the facial tangential stress evolved with the angle γ. It is interesting to note that both the normal stress σ and tangential stress τ under 30 mN and 40 mN is larger than 50 mN (shown in enlarged part), which is associated with scratching depth and pile-up of grooves. Besides, it can be found that the maximum interfacial tangential stress is much larger than normal stress when the angle γ reached about 3π/5. Especially when the applied normal is 30 mN, the maximum interfacial tangential stress approximates 120 GPa. Previous study [31] has testified that 6H-SiC has no high-pressure data beyond 95GPa. A transition to a metallic phase has been observed only in shock compression experiments at a pressure of 105($\pm$4) GPa. However, the maximum normal stress within the chosen normal load during the scratching process is about 48.6 GPa, which is not sufficient to result in amorphization. Therefore, these results indicate that the amorphous phase in ductile debris is determined by interfacial tangential stress rather than normal contact pressure. The dislocation deformation behavior in the substrate of 6H-SiC, however, is mainly dominated by the normal contact pressure. This is the reason why there is no broadband Raman-peak appeared in substrate of 6H-SiC grain. Whereas, the absence

of amorphous phase in fracture chips is due to the fact that the facture chips are induced by the lateral cracks nucleation and propagation, which is not involved in plastic deformation.
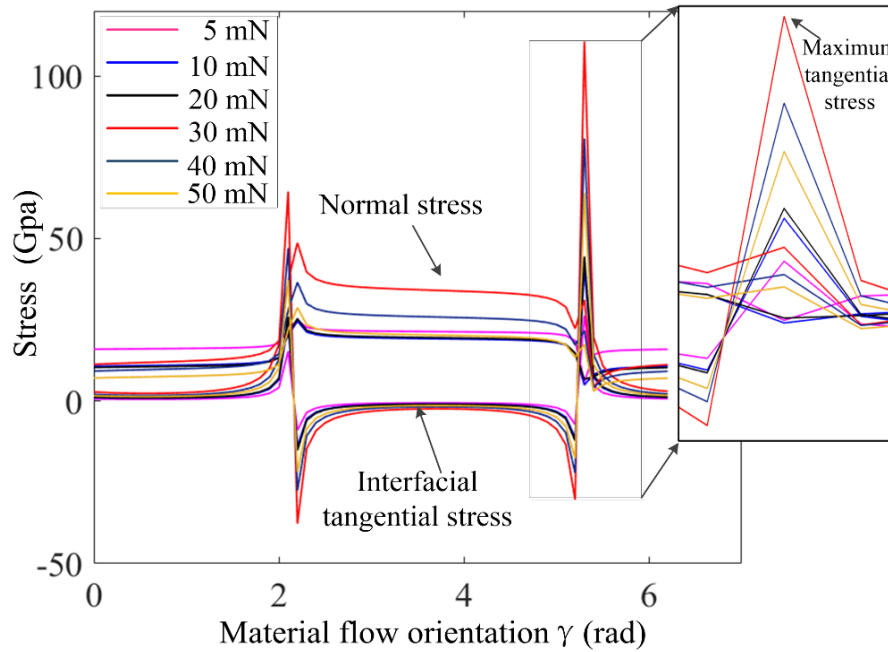
Fig. 6. (a) Normal and tangential stresses acting on the indenter faces as functions of the direction (angle) of the friction on the considered face for RB-SiC ceramic.

3.2 Effect of normal load and scratching velocity on scratch behaviour

In this section, the intent is mainly to analyse the effects of applied normal load and scratching velocity on the residual depth and elastic recovery based on the corresponding deformation mechanism during scratching of RB-SiC ceramic.

The typical 3D topography and cross section of scratch grooves that measured by AFM were illustrated in **Fig. 7**. For increasing normal load case, the residual depth has a significant increase. Besides, it can be found that when normal load reached 30 mN, the split valley appeared within the scratch groove which attribute to the fracture features as presented in **Fig. 4**. To identify the quantitative relationship between the applied normal load and residual depth and elastic recovery, the measured data are plotted against the normal load as shown in **Fig. 8**.

Before choose the suitable fitting function, we must make clear the inner link between the removal behaviour characterize and removal mechanism. Here, according to previous research, we can assume that the scratch depth is proportional to scratch hardness. Scratching hardness is commonly used as an indicator of the inherent material resistance to scratch deformation [22, 32]. It can be obtained through applied normal load F_N on indenter divided by project area A_N as follows [22]:

$$H = k\frac{F_N}{a^2} \tag{7}$$

Where k is the modified coefficient. What's more, the hardness can be written as a simplified function of strain rate which put forward by reference [33]:

$$H = D(\dot{\varepsilon} \tag{8}$$

Where D and m are empirical coefficients, $\dot{\varepsilon}$ is the time derivative of strain, which can be used to characterize the deformation velocity of the material. The strain rate during the scratching process can be calculated by dividing the scratching velocity v by scratch width a as [34]:

$$\dot{\varepsilon} \quad \frac{v}{a} \tag{9}$$

Here, C is a constant expressing the effective strain and introduced to account for the relative strain imposed due to the indenter geometry. Since, the groove width of scratch has a definition relationship with scratch depth for Berkovich indenter, thereby combining Eqs. (7), (8) and (9), it can be deduced as:

$$\frac{F_N}{v^m} \propto a^{2-m} \propto h^n \tag{10}$$

Consequently, it is expected that the trend lines of scratch depth should follow a direct proportion relationship with applied normal force and opposite to scratching velocity. As shown in **Fig. 8a**, the residual depth of scratch grooves and normal force

was best suitable fitted with the linear function, and the variance was equal to 0.9524, which indicated that the fitting results were highly reliable. As shown in Eq. (12), the relationship between elastic recovery and normal force was fitted by power function, and the variance was equal to 0.9565.

$$H_r = 5.62F_N + 41.146 \tag{11}$$

$$E_r = 45.198F_N^{-0.184} \tag{12}$$

From Eq. (11), the fitting results confirmed that the residual depth increased approximated linearly as the normal force increased. Besides, it can be found that the dispersion of data become significant with the increase of normal load (as shown in **Fig. 8a)**, which should be attribute to the deformation transition from ductile to fracture, that is, micro-cracks start to occur in front of the moving indenter, resulting in the instability of the depth ratio. Especially, when the applied normal load was set to 30 mN to 50 mN, severe irregular brittle fracture will be generated as shown in **Fig. 2e** and **f**, which could further lead the residual scratch depth much deeper. Correspondingly, the elastic recovery ratio was decreased with the increase of normal load as shown in **Fig. 8b.** A good agreement between the prediction obtained by Eq. (10) and experimental results calculated by Eq. (12) is observed. This further illustrated that the fracture dominated removal mode gradually with the increase of applied normal load, and the elastic deformation zone will decrease accordingly.
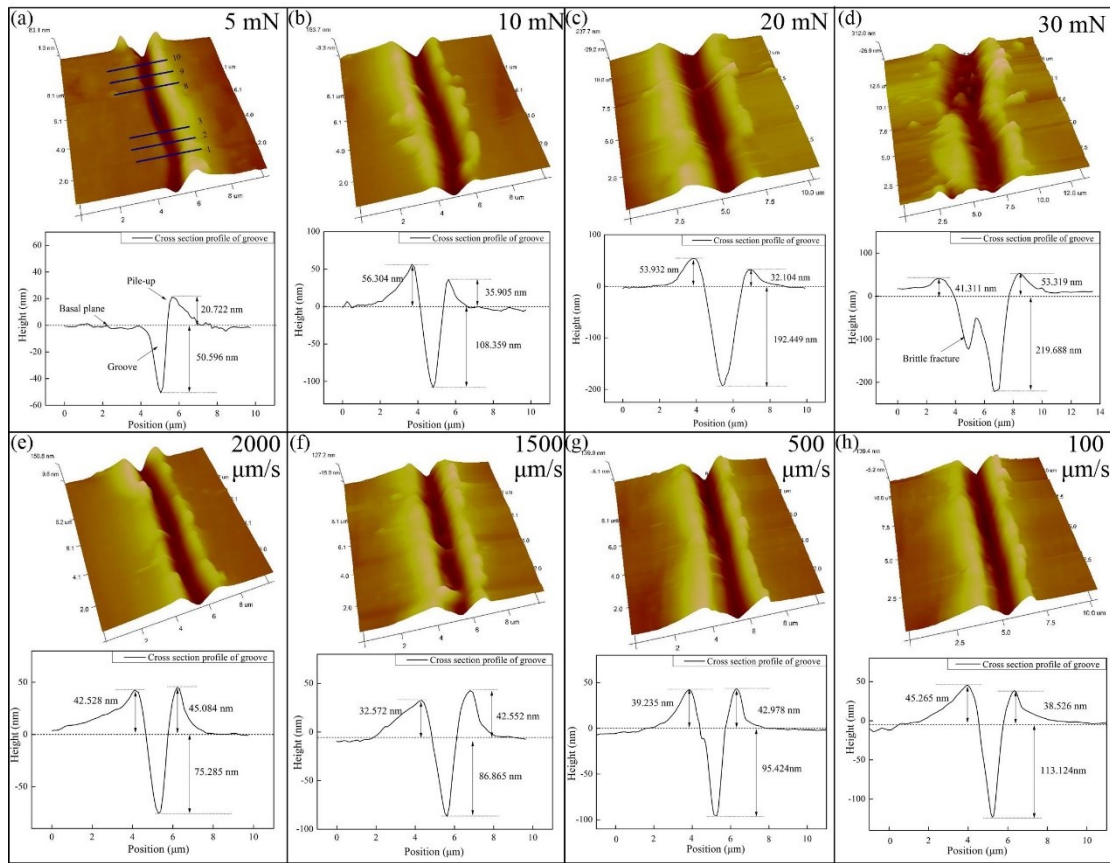
Fig. 7. The typical 3D groove morphology and corresponding cross-section profile measured by AFM.
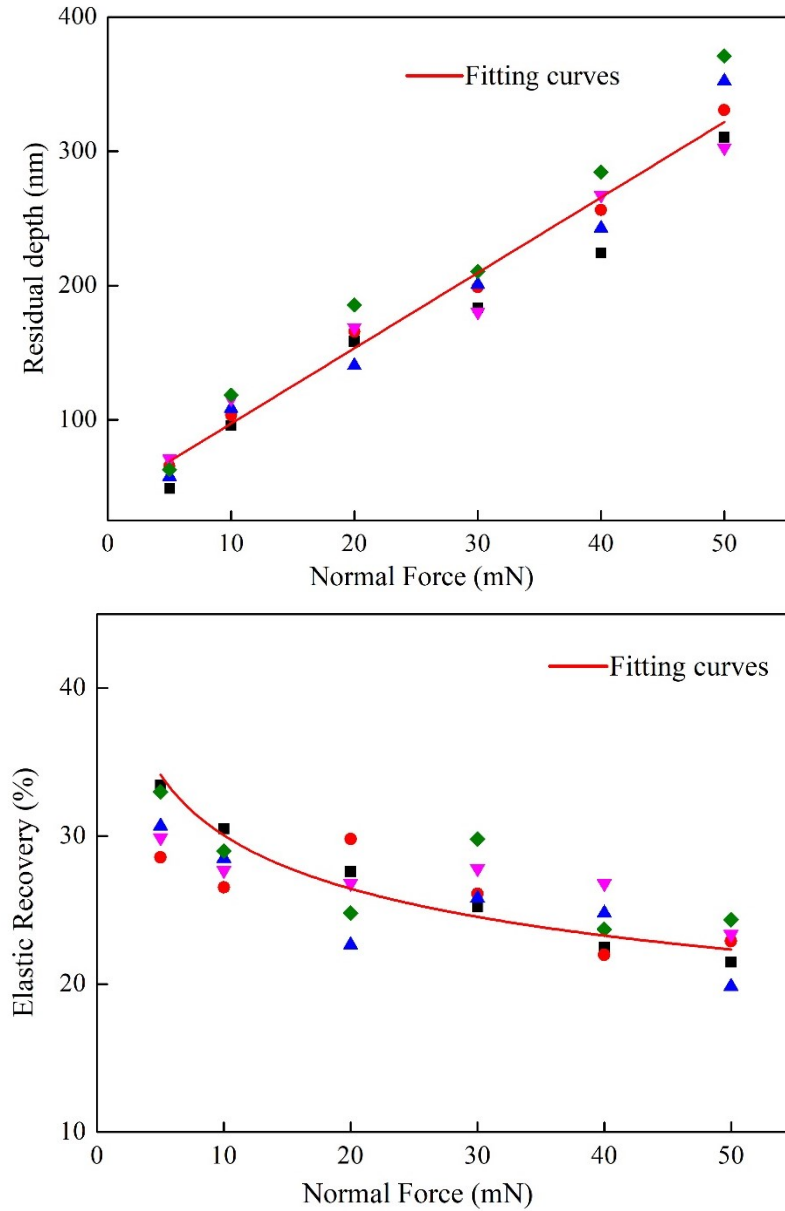
Fig. 8. (a)The residual scratch depth vs. normal load and (b) elastic recovery ratio vs. normal load.

On the other hand, the data of residual depth and elastic recovery vs. scratching velocity were shown in **Fig. 9**. It is evident that residual depth of scratch groove has an opposite trend to the scratching velocity, while the elastic recovery ratio is proportional to the scratching velocity. The empirical formulas fitted for residual depth and elastic recovery vs. scratching velocity were developed as follows:

$$H_r = 97.2834 v^{-0.03684} \tag{13}$$

$$E_r = 27.91e^{0.06671v} \tag{14}$$

The outputs of Eq. (13) demonstrated that the scratch hardness is proportional to scratch velocity, in which the fitting results variance was equal to 0.9759 (**Fig. 9a**). In short, high scratch velocity leads to the increase of resistance to material deformation and final reduce the residual scratch depth. This result can be explained by the dislocation-based plastic deformation mechanism. As mentioned earlier in Section 3.1, ductile mode material removal can be realized when the applied normal load is set to 10 mN. In addition, the substrate deformation response of SiC during ductile process is primary dominated by dislocations as verified by the Raman test. Therefore, it is reasonable to assume that high density of dislocations will be formed and propagated simultaneously with the increase of scratching velocity, which could cause the generation of locks and dislocation tangles. These dislocations prefer to nucleate underneath the indenter, which can hardly assist the plastic removal of 6H-SiC. Instead, this phenomenon will impede propagation of successive mobile dislocations. Hence, the scratch resistance at the contact area where dislocations accumulated was enhanced. On the other hand, the relationship between elastic recovery ratio and scratch velocity follows an exponential function and had a high reliability with the variance is equal to 0.9683 as shown in **Fig. 9b**. This result suggests that as the scratch depth decreases with the increase of scratch velocity, the proportion of elastic deformation also increases, which will further lead to the reduction of residual depth. This finding is especially important for the selection of machining parameters to process hard and brittle materials, and is sounder in explaining the reason of scratch behaviour changes with different scratch velocity.
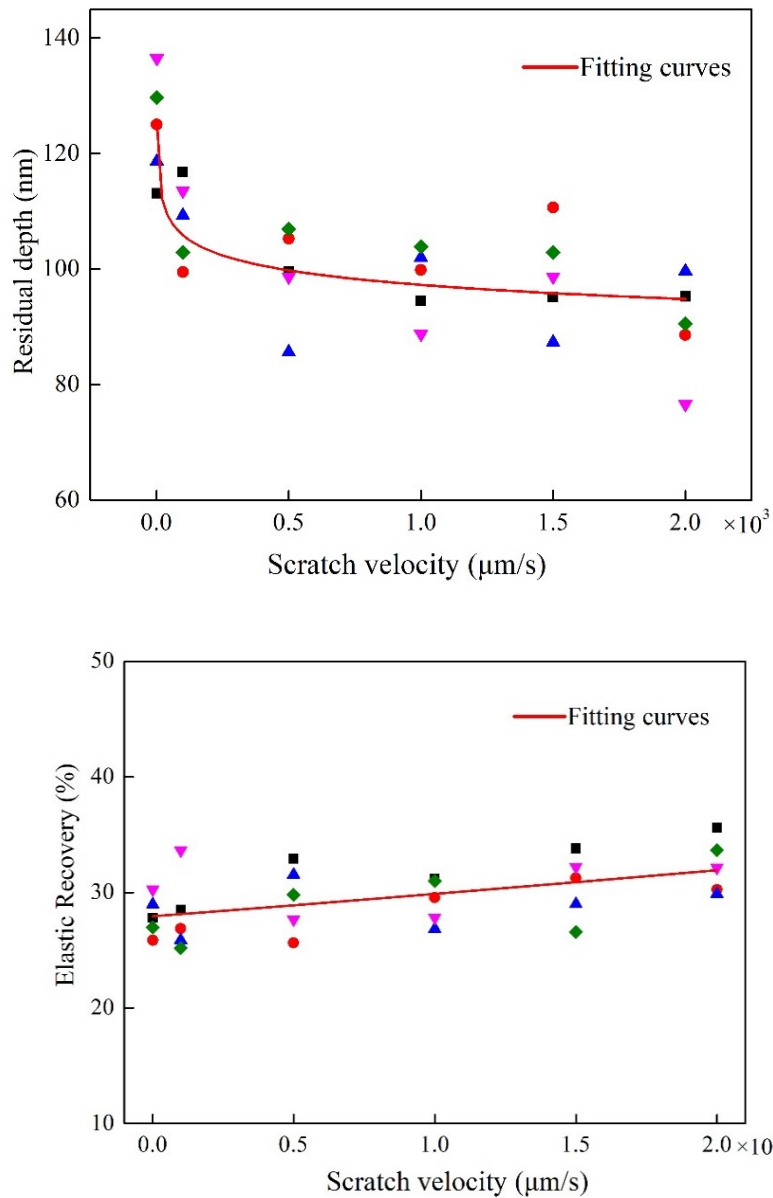
Fig. 9 (a) The residual scratch depth vs. scratching velocity and (b) elastic recovery ratio vs. scratching velocity.

3.3 Effects of normal load and scratching velocity on friction

The aim of this section is to investigate the evolution of friction coefficient in a scratch test with a ramp load mode under different scratching velocity.

Fig. 10 shows a typical scratch friction profile with the increase of applied normal load within the range of 0～50 mN at a given scratching speed of 100 μm/s. It can be seen that the overall friction process can be divided into three stages based on

material deformation characteristics. At the first stage, only the elastic took placed, the surface energy and adhesion of solids in charge of the friction value, which was larger than 1. At the second regime, with the increase of normal load the deformation behavior gradual transited into the elastic-plastic mode. So the adhesion status weakened, and the effect of the ploughing part was increased, which was linked to the deformation of the solids in contact. So the coefficient of friction (COF) dropped rapidly. Besides, the average value of COF under10 mN is about 0.359 (as shown in **Fig. 10**). Such a low coefficient of friction is due to Hexagonal close-packed structure (c/a～1.628), which possess limited number of slip planes as stated in [35]. At last, with the further increase of normal load (24.5 mN), the deformation of RB-SiC enters an unstable stage, in which fracture occurred as presented in **Fig**. **2 and Fig. 4**. From **Fig. 2**, it also should be noted that the grain/phase boundary could contribute to the fluctuation of the friction coefficient. The movements of near surface dislocations in the sliding process are blocked by grain or phase boundary, they accumulated at the grain/phase boundary and produce strain hardening in the surface layer. Hence, this strain hardening makes sliding more difficult and leads to the formation of micro-cracks. As a result, there are some increased peaks emerged on the COF curve as displayed in the insert image of **Fig. 10**.
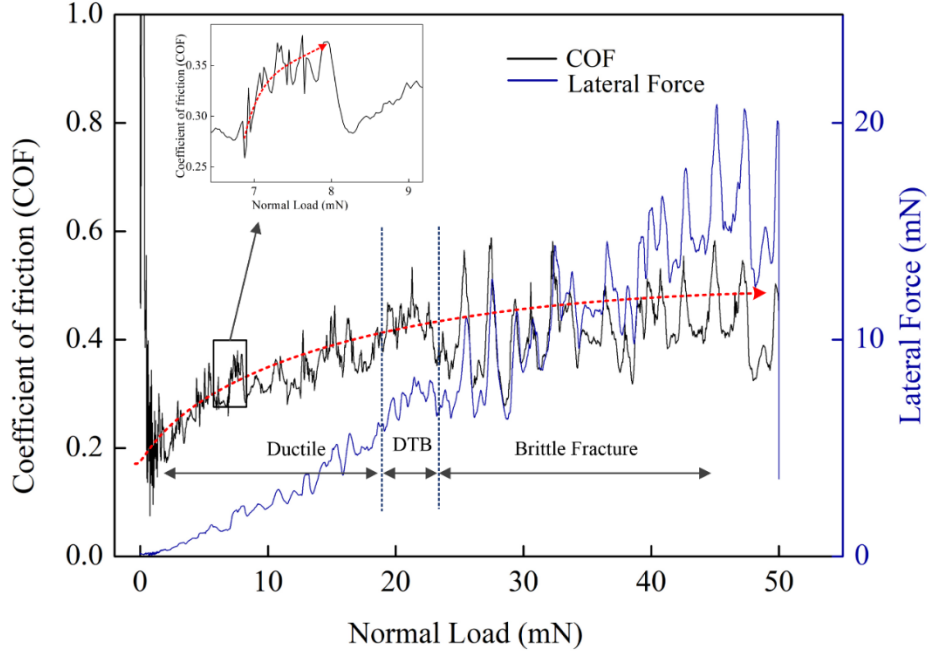
Fig. 10. Typical measured result of friction profile and lateral force for a ramp loading scratch from 0 to 50 mN.

Fig. 11a shows the variations in the average COF with various normal loads of 5～50 mN at a given scratching velocity of 100 μm/s. It clearly shows that the COF increases from 0.358 to 0.51 with the increase of applied normal load. Increased higher intensity of fracture at higher load in the contact region was believed to be responsible for higher friction. **Fig. 11b** shows a drop in the coefficient of friction as a function of scratching velocity. It can be seen that the magnitude of the scratching velocity could alters the overall COF value from 0.332 to 0.425. This fact suggests that the plastic deformation of RB-SiC ceramics is dependent of the strain rate during nanoscratching. Based on Bowden and Tabor's suggestion [36], the overall friction coefficient can be estimated by the sum of two parts, namely, adhesion term μ_a and ploughing term μ_p:

$$\mu = \frac{F_T}{F_N} = \mu_a + \mu_p \qquad (15)$$

Where, the ploughing friction coefficient can be approximated to the ratio of projected area in the scratching direction and projected area in the thrust direction in the contact area:

$$\mu_p \approx \frac{A_P}{A_a} \tag{16}$$

According to the geometrical relationship described in **Section 3.3**, this expression can be rewritten in terms of the angle of γ and α as:

$$\mu_p \approx \frac{\tan\dfrac{\gamma}{2}}{2\sqrt{3}\tan^2\alpha\cos\alpha} \tag{17}$$

From Eq. (17), we can found that the ploughing COF is just related with material flow orientation γ, which is independent of the scratch depth.

Besides, on the basis of reference [37], the adhesion term μ_a can be given by:

$$\mu_a = (\pi/2)(s/\sigma_y) \tag{18}$$

Where s is the effective of shear strength at the interface, σ_y is the yield stress. If we assuming that yielding of the body is isotropic, the compressive yield stress can be expressed by $\sigma_y = \sqrt[3]{H^4/E}$.

Hence, combining Eqs (8), (9) and (18), μ_a can be rewritten as:

$$\mu_a \propto (2/\pi)(s/\sqrt[3]{(v/h)^{4m}/E}) \tag{19}$$

Eq. (19) indicates that the increase of scratching velocity will lead to the increase of compressive stress underneath the indenter, at the end, the dropping of μ_a. The interactions between the high density of dislocations or the impede affection of grain/phase boundary on the mobility of dislocations enhanced the scratch resistant. Therefore, a decrease in percentage reduction of adhesion will result in a decrease of COF, which can be clearly seen in **Fig. 11b**. This result suggests that the COF could be reduced by choosing suitable applied normal load and scratch velocity in the

machining of RB-SiC ceramics. In addition, the fluctuation behavior of COF could reflect the material removal mode during the machining process of RB-SiC ceramics.
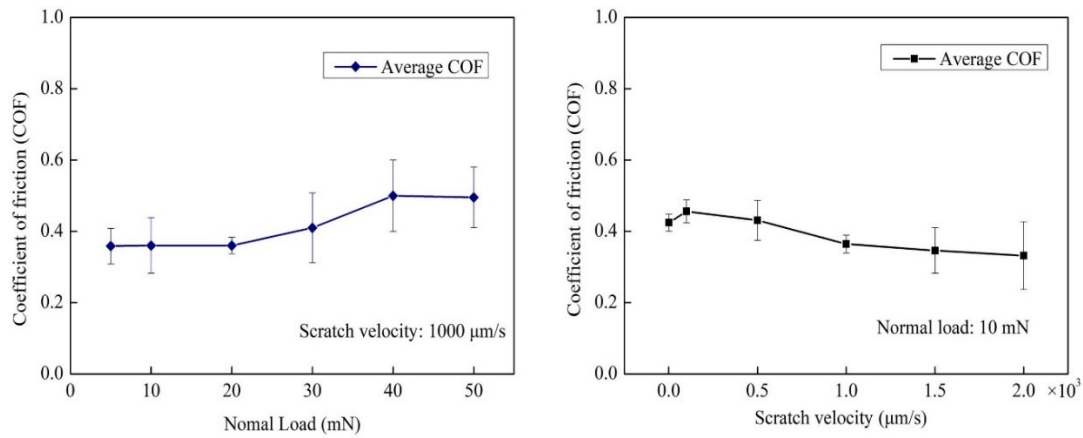
Fig. 11. Coefficient of friction as a function of (a) Normal Load and (b) Scratching velocity.

4. Conclusion

In this paper, a series of nanoscratch experiments followed by SEM, Raman and AFM measurements were performed on RB-SiC ceramic to reveal the material removal mechanism and its effect on the material deformation behavior. The stress underneath the indenter was estimated to analyze the deformation mechanism, which provides an impetus to understand the underlying reason of the different mechanism between ductile chips and substrate within the grooves. The following conclusions can be drawn:

1. Raman spectroscopy revealed that amorphous transformation of SiC and Si occurred in the ductile chips, while amorphous phase absents in the substrate of SiC and brittle fracture chips. The dislocations mobility was the primary response of the ductile deformation in the substrate of SiC. The calculated stress beneath the indenter indicates that the amorphous deformation mechanism in ductile chips and dislocations mobility in subsurface of substrate were governed by the tangential and normal stresses, respectively.

2. The AFM measurement results showed that with the applied normal load increased, the residual scratch depth increased linearly and the elastic recovery decreased follow power law. The residual depth and elastic recovery has a power-law and exponential function relationship with scratching velocity, respectively. The interaction of dislocations accounts for the enhanced scratching hardness with the increase of scratching velocity.

3. The magnitude and the fluctuation of friction coefficient increase with the increase of the applied normal load, which is due to the influence of brittle facture deformation mode. In this process, the grain and phase boundary also contribute to the fluctuation of the friction coefficient. The gradually weakened adhesion coefficient leads to the overall COF decreases with the increase of scratching velocity.

Acknowledgements

References

[1] E. Sein, Y. Toulemont, F. Safa, et al, A Φ 3.5 M SiC telescope for HERSCHEL mission, Proc SPIE. 4850 (2002) 606–618.

[2] J. Robichaud, SiC optics for Earth observing applications, Proc SPIE. 5151 (2003) 53–62.

[3] T.G. Bifano, T.A. Dow, R.O. Scattergood, Ductile-Regime Grinding: A New Technology for Machining Brittle Materials, J Eng Ind. 113 (1991) 184.

[4] E. Brinksmeier, Y. Mutlugünes, F. Klocke, et al, Ultra-precision grinding, CIRP Ann - Manuf Technol. 59 (2010) 652–671.

[5] B. Li, J. Ni, J. Yang, S.Y. Liang, Study on high-speed grinding mechanisms for quality and process efficiency, Int J Adv Manuf Technol. 70 (2014) 813–819.

[6] Z. Wu, W. Liu, L. Zhang, Revealing the deformation mechanisms of 6H-silicon carbide under nano-cutting, Comput Mater Sci. 137 (2017) 282–288.

[7] M. Chen, Q. Zhao, S. Dong, D. Li, The critical conditions of brittle-ductile transition and the factors influencing the surface quality of brittle materials in ultra-precision grinding, J Mater Process Technol. 168 (2005)75–82.

[8] M, Yang, C, Li, Y. Zhang, et al, Maximum undeformed equivalent chip thickness for ductile-brittle transition of zirconia ceramics under different lubrication conditions, Int J Mach Tools Manuf. 122 (2017) 55–65.

[9] D. Zhu, S. Yan, B. Li, Single-grit modeling and simulation of crack initiation and propagation in SiC grinding using maximum undeformed chip thickness, Comput Mater Sci. 92 (2014) 13–21.

[10] J. Cheng, Y.D. Gong, Experimental study on ductile-regime micro-grinding character of soda-lime glass with diamond tool, Int J Adv Manuf Technol. 69 (2013) 147–160.

[11] P. Pirouz, M. Zhang, J.L. Demenet, H.M. Hobgood, Transition from brittleness to ductility in SiC, J Phys Condens Matter. 14 (2002) 12929–12945.

[12] J. Cao, Y. Wu, D. Lu, et al, Material removal behavior in ultrasonic-assisted scratching of SiC ceramics with a single diamond tool, Int J Mach Tools Manuf. 79 (2014) 49–61.

[13] B. Meng, F. Zhang, Z. Li, Deformation and removal characteristics in nanoscratching of 6H-SiC with Berkovich indenter, Mater Sci Semicond Process. 31(2015)160–165.

[14] L. Yin, E.Y.J. Vancoille, K. Ramesh, H. Huang, Surface characterization of

6H-SiC (0001) substrates in indentation and abrasive machining, Int J Mach Tools Manuf. 44 (2004) 607–615.

[15] Q. Zhang, S. To, Q. Zhao, B. Guo, Amorphization and C segregation based surface generation of Reaction-Bonded SiC/Si composites under micro-grinding, Int J Mach Tools Manuf. 95 (2015) 78–81.

[16] G. Xiao, S. To, G. Zhang, The mechanism of ductile deformation in ductile regime machining of 6H SiC, Comput Mater Sci. 98 (2015) 178–188.

[17] J. Yan, Z. Zhang, T. Kuriyagawa, Mechanism for material removal in diamond turning of reaction-bonded silicon carbide, Int J Mach Tools Manuf. 49 (2009) 366–374.

[18] V.I. Levitas, J.A. Patten, High-density amorphous phase of silicon carbide obtained under large plastic shear and high pressure, Phys Rev B. 85 (2012) 054114.

[19] S. Goel, X. Luo, R.L. Reuben, W.B. Rashid, Atomistic aspects of ductile responses of cubic silicon carbide during nanometric cutting, Nanoscale Res Lett. 6 (2011) 1–9.

[20] S. Goel, X. Luo, R.L. Reuben, Shear instability of nanocrystalline silicon carbide during nanometric cutting, Appl Phys Lett. 100 (2012).

[21] B. Meng, Y. Zhang, F. Zhang, Material removal mechanism of 6H-SiC studied by nano-scratching with Berkovich indenter, Appl Phys A Mater Sci Process. 122 (2016) 1–9.

[22] W. Gu, Z. Yao, K. Li, Evaluation of subsurface crack depth during scratch test for optical glass BK7, Proc Inst Mech Eng Part C J Mech Eng Sci. 225 (2011) 2767–2774.

[23] M. Klecka, G. Subhash, Grain size dependence of scratch-induced damage in

alumina ceramics, Wear. 265 (2008) 612–619.

[24] S. Nakashima, H. Harima, Raman investigation of SiC polytypes, Physica Status Solidi a-Applied Research. 162 (1) (1997) 39-64.

[25] S, Nakashima, K. Kisoda, H. Niizuma, H. Harima, Raman scattering of disordered SiC, Physica B: Condensed Matter. 219–220 (1996) 371–373.

[26] Z. Li, F. Zhang, Y. Zhang, X. Luo, Experimental investigation on the surface and subsurface damages characteristics and formation mechanisms in ultra-precision grinding of SiC, Int J Adv Manuf Technol. 92 (2017) 2677–2688.

[27] J.W. Yan, T. Asami, T. Kuriyagawa, Nondestructive measurement of machining-induced amorphous layers in single-crystal silicon by laser micro-Raman spectroscopy, Precis Eng. 32 (3) (2008) 186-195.

[28] J.W. Yan, T. Asami, H. Harada, T. Kuriyagawa, Fundamental investigation of subsurface damage in single crystalline silicon caused by diamond machining, Precis Eng. 33 (4) (2009) 378-386.

[29] F. Zhang, B. Meng, Y. Geng, Y. Zhang, Z. Li, Friction behavior in nanoscratching of reaction bonded silicon carbide ceramic with Berkovich and sphere indenters, Tribology Int. 97 (2016) 21–30.

[30] V. Jardret, H. Zahouani, J.L. Loubet, T.G. Mathia, Understanding and quantification of elastic and plastic deformation during a scratch test, Wear. 218 (1998) 8-14.

[31] M. Yoshida, A. Onodera, M. Ueno, et al, Pressure-induced phase transition in SiC, Phys Rev B. 48 (1994) 10587.

[32] G. Subhash, R. Bandyo, A new scratch resistance measure for structural ceramics, J Am Ceram Soc. 88 (2005) 918–925.

[33] P. Grau, G. Berg, H. Meinhard, S. Mosch, Strain rate dependence of the hardness

of glass and Meyer's law, J. Am. Ceram. Soc. 81 (6) (2010) 1557–1564.

[34] M. Barletta, A. Gisario, L. Lusvarghi, G. Bolelli, G. Rubino, On the combined use of scratch tests and CLA profilometry for the characterization of polyester powder coating: influence of scratch load and speed, Appl Surf Sci. 254 (2008) 7198–7214.

[35] K. Miyoshi, D.H. Buckley, Friction, Deformation and Fracture of Single-Crystal Silicon Carbide, ASLE Trans. 22 (1979) 79–90.

[36] F.P. Bowden, D. Tabor, The friction and lubrication of solids, Oxford University Press, London, 1958.

[37] D.F. Moore, Principles and Applications of Tribology, Oxford Pergamon Press, London, 1975.